Extreme Mechanics Letters 12 (2017) 23–29

Contents lists available at ScienceDirect

Extreme Mechanics Letters

journal homepage: www.elsevier.com/locate/eml

Tunable elastodynamic band gaps

Ellis G. Barnwell, William J. Parnell *, I. David Abrahams *

School of Mathematics, University of Manchester, Oxford Road, Manchester M13 9PL, UK

ARTICLE INFO

Article history:
Received 22 March 2016
Received in revised form
22 October 2016
Accepted 24 October 2016
Available online 8 November 2016

Keywords:
Phononic crystal
Tunable band structure
Configurable phononic material
Phononic switch
Phononic invariance
Nonlinear elasticity
Pre-stress
Small-on-large
Hyperelastic

ABSTRACT

The effect of nonlinear elastic pre-stress on coupled compressional and vertically polarised shear elastic wave propagation in a two-dimensional periodic structure is investigated. The medium consists of cylindrical annuli embedded on a periodic lattice in a uniform host material. An identical inhomogeneous deformation is imposed in each annulus and the theory of small-on-large is used to find the incremental wave equations governing subsequent small-amplitude elastic waves. The plane-wave-expansion method is employed in order to determine the permissable eigenfrequencies. It is found that the application of pre-stress has a significant effect on the band structure, allowing stop bands to be controlled. The sensitivity of the choice of constitutive behaviour is studied and it is shown that the fundamental shear wave mode is largely unchanged for the class of strain energy functions considered here, whereas the compressional mode is considerably more sensitive to this choice.

1. Introduction

Improvements in engineering and technology rely greatly on advanced, complex materials, which often possess intricate microstructure, permitting macroscopic behaviour that is not present in naturally occurring materials. Elastodynamic and acoustic phononic media present a broad range of opportunities for directing waves [1–3] and being able to design these materials carefully in order to enable wave focusing, filtering and directivity is greatly advantageous. Of specific importance is the notion of *tunable*, *configurable* or *re-configurable* phononic media, which have static and dynamic material properties that can be tuned in real time. Such materials have many obvious advantages over media with properties that are fixed upon manufacture. A standard approach is to modify the microstructure and then understand how this modification affects the macroscopic response on a static and dynamic level. A number of opportunities to enable this have been presented. Early work in tuning the *acoustic* response of such media focused on modifying the band gap properties of phononic media by rotating cylinders [4–6].

Several groups have considered using the influence of magnetic or electric fields as a means to perform external control over a crystal [7,8]. In [9], an electric field deforms annular cylinders that are embedded in air, piezoelectric materials are studied in [10–12] and electro-rheological materials in [13]. Thermal effects have also been proposed but the effect is usually fairly weak and so a phase transition effect is usually required [14,15]. These mechanisms for control provide the advantage of a *phononic switch* in such materials. Mechanical mechanisms to create *photonic* switches have also recently been considered, see e.g. [16,17].

It is well-known that nonlinear elastic pre-stress affects the propagation of subsequent linear elastic waves in the medium [18] and this effect has been exploited in order to modify the band-structure of elastodynamic phononic media. In [19,20] an inhomogeneous beam was considered and it was shown that the band structure can be manipulated effectively using pre-stress. It has recently been noted that the response of a nonlinearly elastic material can be extremely sensitive to the choice of constitutive behaviour [21].

An electrical bias has been employed in order to control deformation and hence band gaps in layered and fibre reinforced media [22,23]. Experiments in one dimensional structures were performed by [24]. By making use of numerical simulations, via the finite-element method, the mechanical tunability of three-dimensional structures has also recently been studied [25]. The effect of microstructural buckling of an elastic material was the

* Corresponding authors.
E-mail addresses: ellis.barnwell@gmail.com (E.G. Barnwell), william.parnell@manchester.ac.uk (W.J. Parnell), i.d.abrahams@manchester.ac.uk (I.D. Abrahams).

http://dx.doi.org/10.1016/j.eml.2016.10.009

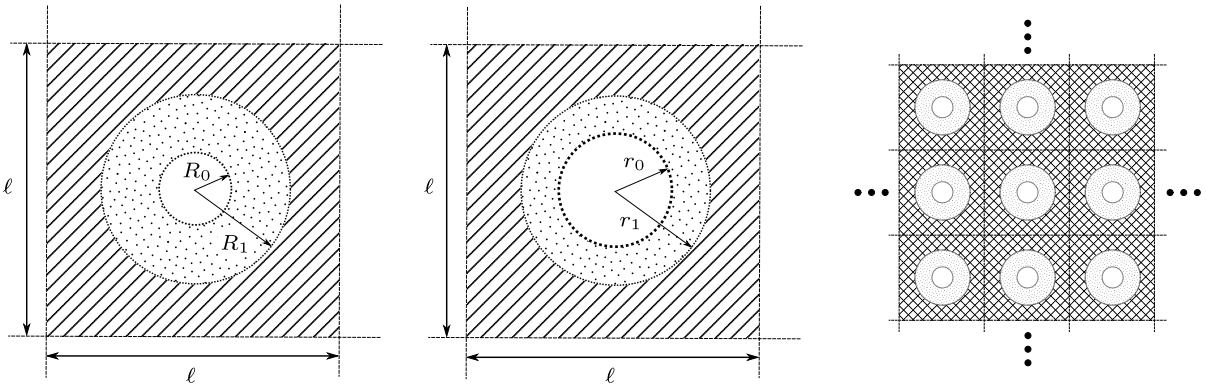

Fig. 1. Illustration of the unit cell for the undeformed configuration on the left and the deformed configuration in the middle. On the right hand side it is shown how the cylindrical annuli are embedded in a square periodic lattice with period ℓ in a stress-free, homogeneous medium shown by the hashed pattern.

focus of investigation in [26–29]. In [30] elastic microstructural helices were employed to control sound.

In this article a new mechanism for the control of band gaps in the full *elastodynamic* context is introduced, based on the work in [31], which was restricted to the scenario of antiplane elastic waves. In that work, incompressible hyperelastic annular cylinders were embedded periodically in an elastic medium and their deformation ensured that band gaps could be switched on and off. Further however, it was shown, based on the theory of hyperelastic cloaking [32–35] that some materials permit deformation in a manner such that in a normal setting from a geometric viewpoint they would possess band gaps but the pre-stress prohibits this; these materials were termed *phononic cloaks*. The theory of *small-on-large* was employed to derive the equations governing the propagation of superposed antiplane elastic waves and the plane-wave-expansion technique was extended in order to accommodate the inhomogeneous deformation present in the cylinders.

Here the same geometry as considered in [31] is employed, as depicted in Fig. 1 but here the annular cylinders are permitted to be *compressible* in order to accommodate the propagation of compressional waves.

2. Deformation and governing incremental wave equations

As illustrated in Fig. 1 the medium consists of a two-dimensional square array (with period ℓ) of nonlinear isotropic elastic annular cylinders each with initial inner and outer radii R_0 and R_1 respectively, density ρ_1 and linear elastic bulk and shear moduli κ_1 and μ_1 respectively, embedded inside a homogeneous elastic host medium of density ρ_0 and linear elastic bulk and shear moduli κ_0 and μ_0. The unit cell is depicted in its stress-free state in Fig. 1(a). All annuli are assumed to be deformed identically. The deformation consists of an inflation (leading to an inhomogeneous radial deformation) and extension along its axis such that, crucially here, the outer radius of the cylinder remains unchanged, $r_1 = R_1$. This results in a deformed configuration as depicted in Fig. 1(b). In principal the host medium can be linear or nonlinearly elastic but here we shall consider it as linear. Subsequent elastodynamic wave propagation depends on the initial deformation and the governing equations are determined by appealing to the theory of small-on-large [18].

It is envisaged that the deformation results from inserting a stiff cylindrical inclusion with elastic properties μ_2 and κ_2 and density ρ_2 into the inner region of the annulus.

2.1. Annular cylinder inflation

The deformation of the annular cylinder is conveniently described in the form

$$R = R(r), \qquad \Theta = \theta, \qquad Z = z/\zeta \tag{1}$$

where the usual convention is followed, using upper (lower) case variables for the reference (deformed) configuration. Deformation is imposed such that

$$R_0 = R(r_0), \qquad R_1 = R(r_1) = r_1. \tag{2}$$

Principal stretches are

$$\lambda_r = \frac{1}{R'(r)}, \qquad \lambda_\theta = \frac{r}{R(r)}, \qquad \lambda_z = \zeta. \tag{3}$$

A second order nonlinear ordinary differential equation (ODE) is determined from the first equation of static equilibrium div$\mathbf{T} = \mathbf{0}$, the second and third being trivially satisfied by the assumed form of deformation. The ODE takes the form

$$R'' = g\left(R, R', W, \zeta\right) \tag{4}$$

where W is the strain energy function governing the constitutive behaviour of the annulus and g is some function that is known only when W is prescribed. This ODE for $R(r)$ is subject to the boundary conditions (2).

In general the ODE (4) cannot be integrated analytically except for six classes of strain energy functions [36]. The issue with these materials types is that they are not considered physically realistic. Therefore two alternative strain energy functions shall be considered here that have been proposed as realistic models of compressible nonlinear elastic materials. First the form introduced by Levinson and Burgess [37] is employed:

$$W_{\mathrm{LB}} = \frac{\mu_1}{2}(I_1 - 3) + \frac{\lambda_1 + \mu_1}{2}(I_3 - 1) - (\lambda_1 + 2\mu_1)(I_3^{1/2} - 1), \tag{5}$$

which was been proposed as a compressible extension of the incompressible neo-Hookean strain energy function and this shall be referred to here as LB. Note that $\lambda_1 = \kappa_1 - 2\mu_1/3$. The second form considered is a compressible extension of the Mooney–Rivlin strain energy function [38]

$$\begin{aligned} W_{\mathrm{CMR}} = {} & \frac{\mu_1 S_1}{2}\left(I_1 - 3 - \log\left(I_3\right)\right) \\ & + \frac{\mu_1(1 - S_1)}{2}\left(I_2 - 3 - 2\log\left(I_3\right)\right) \\ & + \frac{3\lambda_1 + 2\mu_1}{6}\left(I_3^{1/2} - 1\right)^2, \end{aligned} \tag{6}$$

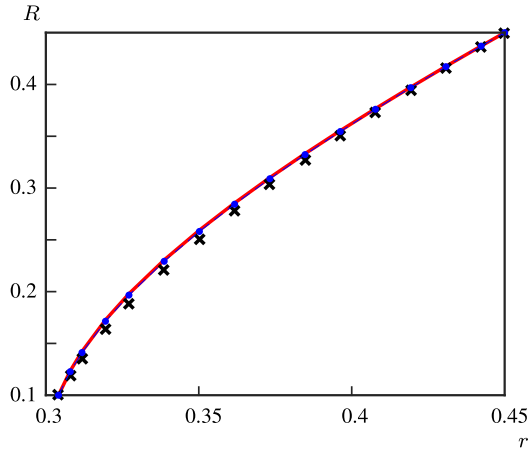

Fig. 2. The deformation of the annulus when it is a Levinson–Burgess (red solid), compressible Mooney–Rivlin ($S_1 = 1$) (blue dashed), and compressible Mooney–Rivlin ($S_1 = 0.6$) (blue dots) material. The incompressible material is shown as black crosses. The initial inner radius is $R_0 = 0.1$, the outer radius is $R_1 = 0.45$ and the axial stretch is $\zeta = 1.4$. The associated volume change is $\Delta V = 0.9$. (For interpretation of the references to colour in this figure legend, the reader is referred to the web version of this article.)

which will be referred to as CMR. Note that W_{CMR} incorporates the I_2 strain invariant and the parameter $S_1 \in [0, 1]$.

The deformation ($R(r)$) is determined numerically within MATLAB by writing the ODE (4) as a system of two first order ODEs, before employing the function bvp4c. The deformation is plotted in Fig. 2. As can be seen, the form of the deformation is largely independent of the choice of strain energy function, and the compressible deformation is only slightly different to the incompressible case. The function $R(r)$ is then used within the incremental equations that govern the propagation of elastodynamic waves.

The deformation is characterised not only by the axial stretch, but also by the volume change given by

$$\Delta V = \frac{V_f}{V_i} = \frac{\zeta(r_1^2 - r_0^2)}{R_1^2 - R_0^2}, \tag{7}$$

where V_i and V_f are the initial and final volumes of the annular section. The deformed inner radius is therefore given by

$$r_0 = \sqrt{R_1^2 - \frac{\Delta V}{\zeta}(R_1^2 - R_0^2)}. \tag{8}$$

For each case, in order to ensure that the annulus is deformed appropriately the necessary radial pressure is applied on the outer surface and the inner expansion is driven by the insertion of the stiff cylindrical inclusion. This is also accompanied by an axial stretch ζ and chosen volume change ΔV. In principal these two parameters can be chosen so that the pressure exerted on the outer boundary of the annulus is zero, which is a more physically satisfying condition in terms of fixing the annuli inside a phononic medium. The annular (nonlinear) region is chosen to be significantly more compliant than the host region and it is assumed that the host material remains stress-free.

2.2. Incremental waves

Assume now that in-plane small-amplitude linear elastic waves propagate through the deformed structure. For geometrical reasons it is convenient to consider the displacements with respect to the cylindrical polar coordinate system and then transform to Cartesian coordinates when quasi-periodicity of the Bloch waves is imposed. In this case, the incremental displacement from the deformed configuration is given by

$$\mathbf{u} = (u_r(r,\theta)\mathbf{e}_r + u_\theta(r,\theta)\mathbf{e}_\theta)e^{-i\omega t}, \tag{9}$$

where $\mathbf{e}_r$ and $\mathbf{e}_\theta$ are unit vectors in the radial and azimuthal directions and where time-harmonic dependence has been assumed; ω is the angular frequency. It is straightforward to show that within the annular cylinder, in the periodic cell, the incremental wave equation is [18]

$$\operatorname{div}\boldsymbol{\zeta} = -\rho_1\,\omega^2\mathbf{u}, \tag{10}$$

where $\boldsymbol{\zeta}$ is the push forward of the incremental nominal stress, given by $\boldsymbol{\zeta} = \mathbf{M} : \boldsymbol{\gamma}$ in which $\boldsymbol{\gamma} = \operatorname{grad}\mathbf{u}$ and

$$M_{ijk\ell} = J^{-1}\frac{\partial^2 W}{\partial F_{jm}\partial F_{\ell n}}F_{im}F_{kn}. \tag{11}$$

It can be shown that (see [18])

$$M_{ijjj} = \frac{\lambda_i\lambda_j}{J}\frac{\partial^2 W}{\partial\lambda_i\partial\lambda_j}, \tag{12}$$

with no sum over repeated indices. Furthermore, provided that $i \neq j$ and $\lambda_i \neq \lambda_j$

$$M_{ijij} = \frac{\lambda_i^2}{J(\lambda_i^2 - \lambda_j^2)}\left(\lambda_i\frac{\partial W}{\partial\lambda_i} - \lambda_j\frac{\partial W}{\partial\lambda_j}\right), \tag{13}$$

$$M_{ijji} = \frac{\lambda_i\lambda_j}{J(\lambda_i^2 - \lambda_j^2)}\left(\lambda_j\frac{\partial W}{\partial\lambda_i} - \lambda_i\frac{\partial W}{\partial\lambda_j}\right). \tag{14}$$

All other combinations give $M_{ijk\ell} = 0$. In the host and inclusion media the governing wave equations are those of linear isotropic elastodynamics with isotropic elastic moduli κ_0, μ_0 and κ_2, μ_2 and densities ρ_0 and ρ_2 respectively. It transpires that for the study of in-plane waves there are four non-zero elements of $\boldsymbol{\zeta}$ that are of interest, which are

$$\begin{aligned}
\zeta_{rr} &= M_{rrrr}\gamma_{rr} + M_{rr\theta\theta}\gamma_{\theta\theta},\\
\zeta_{r\theta} &= M_{r\theta r\theta}\gamma_{\theta r} + M_{r\theta\theta r}\gamma_{r\theta},\\
\zeta_{\theta r} &= M_{\theta r\theta r}\gamma_{r\theta} + M_{\theta rr\theta}\gamma_{\theta r},\\
\zeta_{\theta\theta} &= M_{\theta\theta rr}\gamma_{rr} + M_{\theta\theta\theta\theta}\gamma_{\theta\theta}.
\end{aligned}$$

The stress ζ_{zz} is non-zero but does not influence the propagation of in-plane waves. The following two incremental wave equations are generated:

$$\begin{aligned}
&\frac{\partial}{\partial r}\left(M_{rrrr}\frac{\partial u_r}{\partial r} + M_{rr\theta\theta}\frac{1}{r}\left(\frac{\partial u_\theta}{\partial\theta} + u_r\right)\right)\\
&\quad + \frac{1}{r}\left[\frac{\partial}{\partial\theta}\left(M_{\theta r\theta r}\frac{1}{r}\left(\frac{\partial u_r}{\partial\theta} - u_\theta\right) + M_{\theta rr\theta}\frac{\partial u_\theta}{\partial r}\right)\right.\\
&\quad \left. + (M_{rrrr} - M_{\theta\theta rr})\frac{\partial u_r}{\partial r} + (M_{rr\theta\theta} - M_{\theta\theta\theta\theta})\frac{1}{r}\left(\frac{\partial u_\theta}{\partial\theta} + u_r\right)\right]\\
&\quad + \rho_1\,\omega^2 u_r = 0,
\end{aligned} \tag{15}$$

$$\begin{aligned}
&\frac{\partial}{\partial r}\left(M_{r\theta r\theta}\frac{\partial u_\theta}{\partial r} + M_{r\theta\theta r}\frac{1}{r}\left(\frac{\partial u_r}{\partial\theta} - u_\theta\right)\right)\\
&\quad + \frac{1}{r}\left[\frac{\partial}{\partial\theta}\left(M_{\theta\theta rr}\frac{\partial u_r}{\partial r} + M_{\theta\theta\theta\theta}\frac{1}{r}\left(\frac{\partial u_\theta}{\partial\theta} + u_r\right)\right)\right.\\
&\quad \left. + (M_{r\theta r\theta} + M_{\theta rr\theta})\frac{\partial u_\theta}{\partial r} + (M_{\theta r\theta r} + M_{r\theta\theta r})\frac{1}{r}\left(\frac{\partial u_r}{\partial\theta} - u_\theta\right)\right]\\
&\quad + \rho_1\,\omega^2 u_\theta = 0.
\end{aligned} \tag{16}$$

In order to study Bloch–Floquet wave propagation through the deformed periodic structure, it is now necessary to transform (10)

into Cartesian form. In other words since this is already in "invariant" form, the Cartesian forms of the tensor $\boldsymbol{\zeta}$ must simply be deduced when written in terms of Cartesian displacement components, i.e. $\mathbf{u} = u\mathbf{e}_x + v\mathbf{e}_y$ so that $\boldsymbol{\gamma} = \text{grad}\mathbf{u}$. Upon carrying out this transformation it can be shown that

$$\zeta_{xx} = M_{xxxx}\gamma_{xx} + M_{xxxy}\gamma_{yx} + M_{xxyx}\gamma_{xy} + M_{xxyy}\gamma_{yy}, \tag{17}$$
$$\zeta_{xy} = M_{xyxx}\gamma_{xx} + M_{xyxy}\gamma_{yx} + M_{xyyx}\gamma_{xy} + M_{xyyy}\gamma_{yy}, \tag{18}$$
$$\zeta_{yx} = M_{yzxx}\gamma_{xx} + M_{yxxy}\gamma_{yx} + M_{yxyx}\gamma_{xy} + M_{yxyy}\gamma_{yy}, \tag{19}$$
$$\zeta_{yy} = M_{yyxx}\gamma_{xx} + M_{yyxy}\gamma_{yx} + M_{yyyx}\gamma_{xy} + M_{yyyy}\gamma_{yy} \tag{20}$$

where $M_{ijk\ell}$ given here with respect to the Cartesian basis are specified in terms of their cylindrical coordinate system counterparts in the Appendix.

3. Implementation of the modified plane-wave-expansion technique

The implementation of the plane-wave-expansion method is carried out in much the same manner as described in [31] expect that here instead of a scalar problem, the pair of coupled Eqs. (15)–(16) governing the (coupled) shear and pressure waves must be dealt with. First, the reciprocal lattice is introduced:

$$\mathbf{G} = \frac{2\pi}{\ell}(m\mathbf{e}_x + n\mathbf{e}_y) \tag{21}$$

where m, n span the integers. Introducing the Bloch wave vector $\mathbf{K}$, displacements are written in the quasi-periodic form

$$u(\mathbf{x}) = e^{i\mathbf{K}\cdot\mathbf{x}} \sum_{\mathbf{G}} U[\mathbf{G}]\, e^{i\mathbf{G}\cdot\mathbf{x}}, \tag{22}$$
$$v(\mathbf{x}) = e^{i\mathbf{K}\cdot\mathbf{x}} \sum_{\mathbf{G}} V[\mathbf{G}]\, e^{i\mathbf{G}\cdot\mathbf{x}}, \tag{23}$$

noting that the sum here is a double sum over m and n (spanning all integers). The (periodic) incremental moduli are written in (periodic) plane-wave form, e.g.

$$M_{xxxx}(\mathbf{x}) = \sum_{\mathbf{G}} m_{xxxx}[\mathbf{G}]e^{i\mathbf{G}\cdot\mathbf{x}} \tag{24}$$

and analogously for all other $M_{ijk\ell}$ and the density $\rho(\mathbf{x})$ with plane-wave (Fourier) coefficients $m_{ijk\ell}[\mathbf{G}]$ and $\mathcal{R}[\mathbf{G}]$ respectively.

Using (22)–(23) as well as the material property expansions such as (24) in the governing equations with the forms (17)–(20) generates an infinite homogeneous linear system for the components $U[\mathbf{G}]$ and $V[\mathbf{G}]$. Truncating the sum over plane waves gives a finite system of the form

$$(A[K_x, K_y] + \omega^2 B)\,\mathcal{U}[\mathbf{G}] = 0 \tag{25}$$

where, having truncated the system with m and n ranging from $-N_{\max}$ to $N_{\max}$, the vector $\mathcal{U}[\mathbf{G}]$ is written in the short-hand form

$$\mathcal{U}[\mathbf{G}] = \begin{pmatrix} U[-N_{\max}, -N_{\max}] \\ U[-N_{\max}+1, -N_{\max}] \\ \vdots \\ U[N_{\max}, N_{\max}] \\ V[-N_{\max}, -N_{\max}] \\ V[-N_{\max}+1, -N_{\max}] \\ \vdots \\ V[N_{\max}, N_{\max}] \end{pmatrix}. \tag{26}$$

It should also be noted that B depends only on the Fourier coefficients of the density, i.e. $\mathcal{R}[\mathbf{G}]$. The matrix eigenvalue problem (25) is solved using the MATLAB `eig` function and this enables the dispersion relation $\mathbf{K} = \mathbf{K}(\omega)$ to be determined.

4. Tuning band gaps: results

When presenting results associated with dispersion relations, the band diagrams will be plotted in the usual manner. That is, the frequency of each mode is determined whilst scanning the wavenumber around the edge of the irreducible Brillouin zone [39,2]. Following convention, the three points defining this boundary are denoted Γ ($\hat{\mathbf{K}} = 0\mathbf{i} + 0\mathbf{j}$), X ($\hat{\mathbf{K}} = 0.5\mathbf{i} + 0\mathbf{j}$) and M ($\hat{\mathbf{K}} = 0.5\mathbf{i} + 0.5\mathbf{j}$).

Throughout the results section, the Lamé parameters and density are non-dimensionalised on those of the host material and the wavenumbers on the lattice period ℓ, i.e. for $j = 0, 1, 2$

$$\hat{\mu}_j = \frac{\mu_j}{\mu_0}, \qquad \hat{\lambda}_j = \frac{\lambda_j}{\mu_0} \qquad \hat{\rho}_j = \frac{\rho_j}{\rho_0},$$
$$\hat{\mathbf{K}} = \ell\mathbf{K}, \qquad \hat{\mathbf{G}} = \ell\mathbf{G}. \tag{27}$$

The nondimensional frequency therefore becomes

$$\hat{\omega} = \frac{\ell\omega}{c_0}, \tag{28}$$

where $c_0 = \sqrt{\mu_0/\rho_0}$ is the shear wave speed in the host material (and unstressed annulus due to the choice of properties above). The spatial variable is non-dimensionalised on the period, ℓ, i.e. $\hat{x} = \frac{x}{\ell}$, $\hat{y} = \frac{y}{\ell}$, and so the unit cell is mapped to the region $-1/2 < \hat{x} < 1/2$ and $-1/2 < \hat{y} < 1/2$. The outer radius of the pre-stressed region remains fixed at $R_1 = r_1 = 0.45$. This value was chosen since it is large enough to give a sizeable pre-stressed region, but not too large so the pre-stressed region is close to the outer edge of the unit cell. Although it is possible to study the latter case as r_1 gets closer to 0.5, a significant increase in the number of terms in the PWE is required. Since this is not the main focus of the study it is avoided here.

For all calculations, the maximum plane-wave number is taken at $N_{\max} = 10$ (corresponding to 441 plane waves) which has been established to give sufficiently accurate results. The percentage error in the method is estimated by taking a large number of plane waves and is typically below 0.05%.

Through the remainder of this paper, the non-dimensional properties in the host region and annulus are chosen to be $\hat{\mu}_0 = \hat{\mu}_1 = 1$, $\hat{\lambda}_0 = \hat{\lambda}_1 = 2$ and $\hat{\rho}_0 = \hat{\rho}_1 = 1$. For the inclusion, the material properties are chosen to be stiffer and denser: $\hat{\mu} = 5$, $\hat{\lambda} = 30$ and $\hat{\rho} = 2$ in this region.

4.1. P-SV mode

In Fig. 3 the effect on the band diagram associated with the coupled compressional/vertically polarised shear waves is illustrated after applying a pre-stress of the form described in Section 2.1 with $\zeta = 1.4$ and volume change $\Delta V = 0.8$ for the LB and CMR materials. A significant change in the band diagram is observed including the appearance of an absolute band gap for the coupled mode. However, when compared to the band diagram of a stress free material with larger inclusion (with radius equal to the inner annulus radius in the deformed state), the stress free material exhibits a significantly larger band gap. This means that materials can be generated in a pre-stressed that permit the propagation of elastodynamic waves in frequency ranges that are not possible in unstressed media with the same geometry.

It is appears that altering the Mooney–Rivlin parameter has no significant effect on the shape of the band structure. However, the frequencies of the bands are altered slightly, illustrating some sensitivity to choice of material.

In Fig. 4 the effective (fundamental) shear and compressional wavespeeds are plotted and band gap widths for the various materials. In these plots, typical values of the pre-stress are chosen as

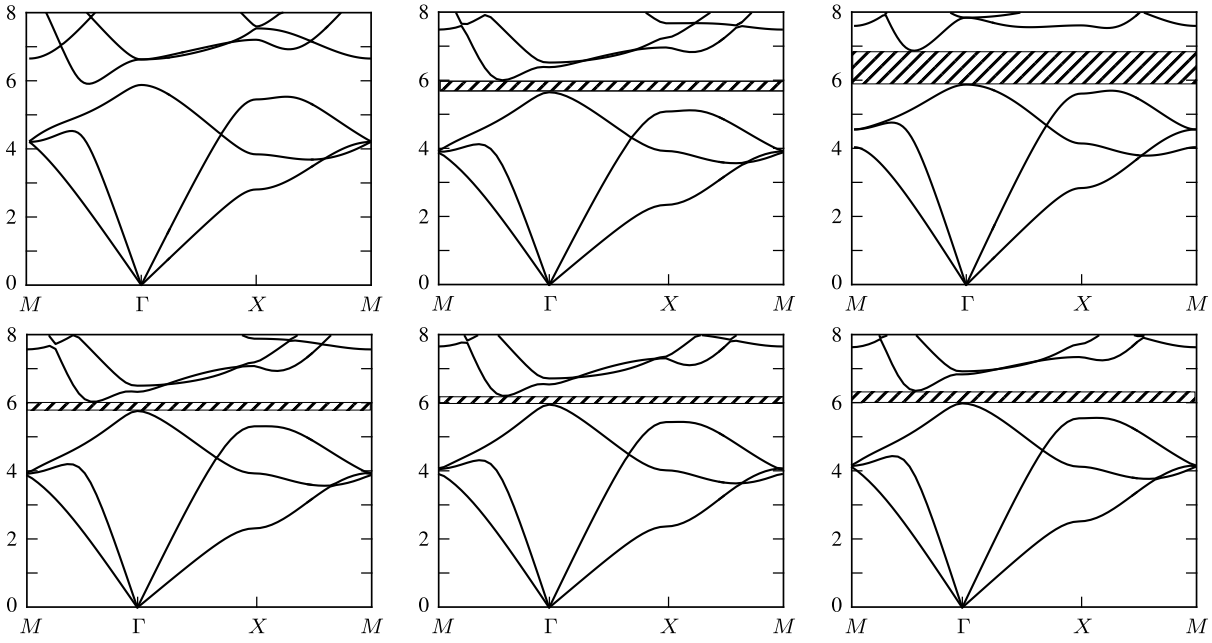

Fig. 3. Band diagrams for a number of different materials. The top left figure is a stress free solid with inclusions of size $R_0 = r_0 = 0.275$, the top middle is a pre-stressed Levinson–Burgess strain energy function, the top right is a stress free solid with inclusion size $R_0 = 0.36$ and the bottom three diagrams are compressible Mooney–Rivlin materials with (from left to right) $S_1 = 1$, $S_1 = 0.8$ and $S_1 = 0.6$. All of the pre-stressed materials have initial radius $R_0 = 0.3$, axial stretch $\zeta = 1.4$ and volume change $\Delta V = 0.8$. Stop bands are indicated by the shaded regions.

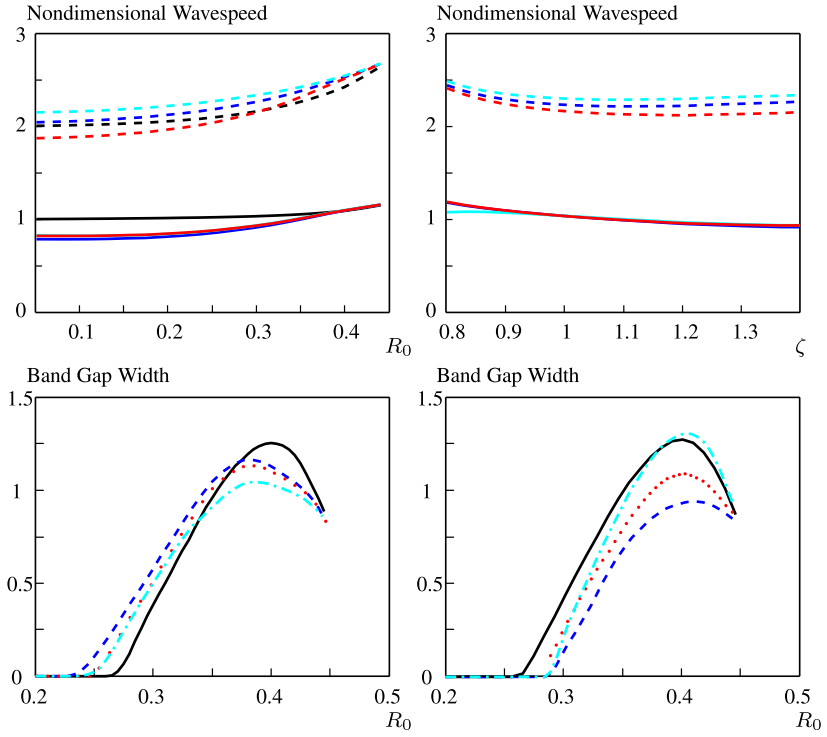

Fig. 4. The effective wavespeed of the fundamental modes for the pre-stressed periodic structure is shown in the upper two figures. With variation in the undeformed inner radius (left) and with variation of the axial stretch (right, with $\Delta V = 1/\zeta$). The shear mode is shown by the solid line and the compressional mode by the dashed line. Results are shown for stress free (black), LB (red), CMR $S_1 = 1$ (dark blue) and CMR $S_1 = 0.6$ (light blue). The lower two figures show the band gap width as a function of undeformed radius. On the left is stress free (solid) LB (dashed blue), CMR $S_1 = 1$ (dotted red) and CMR $S_1 = 0.6$ (dot dash blue). On the right, the width for no axial stretch ($\zeta = 1$) is shown where $\Delta V = 1$ (no pre-stress, solid), $\Delta V = 0.8$ (dashed blue), $\Delta V = 0.6$ (dotted red) and $\Delta V = 1.2$ (dot dash light blue). (For interpretation of the references to colour in this figure legend, the reader is referred to the web version of this article.)

$\zeta = 1.4$ and $\Delta V = 0.8$ and the typical inner radius is chosen as $R_0 = 0.3$.

All materials show generally the same trends with regards to the wavespeed. Although the shear wavespeed for the different materials is largely unchanged, the choice of material properties has a significant effect on the compressional wavespeed. This shows a sensitivity to the strain energy function that is not initially obvious from the band diagrams.

It is clear that there is some dependence of the band gap width on the strain energy function. However, rather interestingly

all strain energy functions cause the band gap to be switched on at a smaller initial radius than would occur in an initially unstressed medium. It is also interesting to note that applying differing amounts of compression, and keeping $\zeta = 1$, has a large effect on the width of the stop band but does not change the point at which the stop band switches on. The $\zeta = 1$ case is of specific interest since this means that the annulus could be held in situ within the material when imposing initial pre-stress.

5. Concluding remarks

In this paper the theory of small-on-large has been employed to incorporate pre-stress into a phononic crystal made up of a compressible elastic material. The effect of this pre-stress on the band structure was investigated for two different strain energy functions.

For the coupled pressure and shear mode we have shown that applying pre-stress can have the effect of switching on and off stop bands, giving a mechanism for real time tuning. The sensitivity to different strain energy functions was investigating and it was shown that in some situations the choice of constitutive behaviour has a significant effect on the material response. This effect is more pronounced for the compressional wave mode than the shear mode.

There is scope for future work influenced by the work given here. In particular, it would be interesting to include the SH mode to see if it is possible to create an absolute band gap for all modes. Similarly, it would be interesting to determine if it is possible to obtain a stop band in the pressure mode but allow the same frequencies to propagate in the shear mode. In doing this, by building a finite specimen it may be possible to convert pressure waves from a fluid into shear waves in a (phononic) solid, thus making efficient soundproofing at specific frequencies.

Acknowledgements

The authors acknowledge the Leverhulme Trust for financial support via grant F/00120/CC, which funded the Ph.D. studentship of Barnwell. Parnell is grateful to the Engineering and Physical Sciences Research Council for funding his fellowship (EP/L018039/1) and Abrahams thanks the Royal Society for a Wolfson Research Merit award (2013–2018).

Appendix. Incremental moduli in Cartesian form

$$M_{xxxx} = \frac{1}{r^4}\left[x^4 M_{rrrr} + y^4 M_{\theta\theta\theta\theta} + x^2y^2(2M_{rr\theta\theta} + 2M_{r\theta\theta r} + M_{r\theta r\theta} + M_{\theta r\theta r})\right],$$

$$M_{xxyy} = M_{yyxx} = \frac{1}{r^4}\left[x^4 M_{rr\theta\theta} + y^4 M_{\theta\theta rr} + x^2y^2(M_{rrrr} - M_{r\theta r\theta} - 2M_{r\theta\theta r} - M_{\theta r\theta r} + M_{\theta\theta\theta\theta})\right],$$

$$M_{xxxy} = M_{xyxx} = \frac{xy}{r^4}\left[x^2(M_{rrrr} - M_{rr\theta\theta} - M_{r\theta r\theta} - M_{r\theta\theta r}) + y^2(M_{r\theta\theta r} + M_{\theta r\theta r} - M_{\theta\theta\theta\theta} + M_{rr\theta\theta})\right],$$

$$M_{xxyx} = M_{yxxx} = \frac{xy}{r^4}\left[x^2(M_{rrrr} - M_{\theta r\theta r} - M_{r\theta\theta r} - M_{rr\theta\theta}) + y^2(M_{rr\theta\theta} + M_{r\theta r\theta} + M_{r\theta\theta r} - M_{\theta\theta\theta\theta})\right],$$

$$M_{xyxy} = \frac{1}{r^4}\left[x^4 M_{r\theta r\theta} + y^4 M_{\theta r\theta r} + x^2y^2(M_{rrrr} - 2M_{rr\theta\theta} - 2M_{r\theta\theta r} + M_{\theta\theta\theta\theta})\right],$$

$$M_{xyyx} = M_{yxxy} = \frac{xy}{r^4}\left[x^2(M_{r\theta r\theta} + M_{r\theta r\theta} - M_{\theta\theta\theta\theta} + M_{\theta\theta rr}) + y^2(M_{rrrr} - M_{rr\theta\theta} - M_{r\theta\theta r} - M_{\theta r\theta r})\right],$$

$$M_{xyyy} = M_{yyxy} = \frac{xy}{r^4}\left[x^2(M_{rr\theta\theta} + M_{r\theta r\theta} + M_{r\theta\theta r} - M_{\theta\theta\theta\theta}) + y^2(M_{rrrr} - M_{\theta r\theta r} - M_{r\theta\theta r} - M_{\theta\theta rr})\right],$$

$$M_{xyyx} = M_{yxxy} = \frac{xy}{r^4}\left[x^2(M_{r\theta r\theta} + M_{r\theta r\theta} - M_{\theta\theta\theta\theta} + M_{\theta\theta rr}) + y^2(M_{rrrr} - M_{rr\theta\theta} - M_{r\theta\theta r} - M_{\theta r\theta r})\right],$$

$$M_{yxyx} = \frac{1}{r^4}\left[x^4 M_{\theta r\theta r} + y^4 M_{r\theta r\theta} + x^2y^2(M_{rrrr} - 2M_{rr\theta\theta} - 2M_{r\theta\theta r} + M_{\theta\theta\theta\theta})\right],$$

$$M_{yyyy} = \frac{1}{r^4}\left[x^4 M_{\theta\theta\theta\theta} + y^4 M_{rrrr} + x^2y^2(2M_{rr\theta\theta} + 2M_{r\theta\theta r} + M_{r\theta r\theta} + M_{\theta r\theta r})\right].$$

References

[1] R. Craster, S. Guenneau, Acoustic Metamaterials: Negative Refraction, Imaging, Lensing and Cloaking, Springer, 2013.
[2] P. Deymier, Acoustic Metamaterials and Phononic Crystals, Springer, 2013.
[3] M.I. Hussein, M.J. Leamy, M. Ruzzene, Dynamics of phononic materials and structures: Historial origins, recent progress and future outlook, Appl. Mech. Rev. 66 (2014) 040802.
[4] C. Goffaux, J.P. Vigneron, Theoretical study of a tunable phononic band gap system, Phys. Rev. B: Condens. Matter Mater. Phys. 64 (7) (2001) 5118–5122.
[5] X. Li, F. Wu, H. Hu, S. Zhong, Y. Liu, Large acoustic band gaps created by rotating square rods in two-dimensional periodic composites, J. Phys. D: Appl. Phys. 36 (1) (2003) 15–17.
[6] S.C.S. Lin, T.J. Huang, Tunable phononic crystals with anisotropic inclusions, Phys. Rev. B: Condens. Matter Mater. Phys. 83 (17) (2011) 4303–4312.
[7] O.B. Matar, J.F. Robillard, J.O. Vasseur, A.C. Hladky-Hennion, P.A. Deymier, P. Pernod, V. Preobrazhensky, Band gap tunability of magneto-elastic phononic crystal, J. Appl. Phys. 111 (5) (2012) 4901–4915.
[8] J.Y. Yeh, Control analysis of the tunable phononic crystal with electrorheological material, Physica B 400 (1) (2007) 137–144.
[9] W. Yang, L. Chen, The tunable acoustic band gaps of two-dimensional phononic crystals with a dielectric elastomer cylindrical actuator, Smart Mater. Struct. 17 (2008) 015011.
[10] Z. Hou, F. Wu, Y. Liu, Phononic crystals containing piezoelectric material, Solid State Commun. 130 (11) (2004) 745–749.
[11] X.Y. Zou, Q. Chen, B. Liang, J.C. Cheng, Control of the elastic wave bandgaps in two-dimensional piezoelectric periodic structures, Smart Mater. Struct. 17 (1) (2008) 5008–5012.
[12] F. Casadei, T. Delpero, A. Bergamini, P. Ermanni, M. Ruzzene, Piezoelectric resonator arrays for tunable acoustic waveguides and metamaterials, J. Appl. Phys. 112 (6) (2012) 4902–4906.
[13] X. Zhou, C. Chen, Tuning the locally resonant phononic band structures of two-dimensional periodic electroactive composites, Physica B 431 (1) (2013) 23–31.
[14] Z.G. Huang, T.T. Wu, Temperature effect on bandgaps of surface and bulk acoustic waves in two-dimensional phononic crystals, IEEE Trans. Ultrason. Ferroelectr. Freq. Control 52 (3) (2005) 365–370.
[15] K.L. Jim, C.W. Leung, S.T. Lau, S.H. Choy, H.L.W. Chan, Thermal tuning of phononic bandstructure in ferroelectric ceramic/epoxy phononic crystal, Appl. Phys. Lett. 94 (19) (2009) 3501–3503.
[16] J.Y. Ou, E. Plum, L. Jiang, N.I. Zheludev, Reconfigurable photonic metamaterials, Nano Lett. 11 (2011) 2142–2144.
[17] W. Zhu, Y. Huang, I.D. Rukhlenko, G. Wen, M. Premaratnel, Configurable metamaterial absorber with pseudo wideband spectrum, Opt. Express 20 (6) (2012) 6616–6621.
[18] M. Destrade, G. Saccomandi, Waves in Nonlinear Pre-Stressed Materials, Springer, New York, 2007.

[19] W.J. Parnell, Effective wave propagation in a pre-stressed nonlinear elastic composite bar, J. Appl. Math. 72 (2) (2007) 223–244.
[20] M. Gei, A.B. Movchan, D. Bigoni, Band-gap shift and defect induced annihilation in prestressed elastic structures, J. Appl. Phys. 105 (6) (2009) 3507–3513.
[21] G. Puglisi, G. Saccomandi, Multi-scale modelling of rubber-like materials and soft tissues: an appraisal, Proc. R. Soc. Lond. Ser. A Math. Phys. Eng. Sci. 472 (2187) (2016) 20160060.
[22] G. Shmuel, G. deBotton, Band-gaps in electrostatically controlled dielectric laminates subjected to incremental shear motions, J. Mech. Phys. Solids 60 (11) (2012) 1970–1981.
[23] G. Shmuel, Electrostatically tunable band gaps in finitely extensible dielectric elastomer fiber composites, Internat. J. Solids Struct. 50 (5) (2013) 680–686.
[24] R. Feng, K. Liu, Tuning the band-gap of phononic crystals with an initial stress, Physica B 407 (12) (2012) 2032–2036.
[25] L. Wang, K. Bertoldi, Mechanically tunable phononic band gaps in three-dimensional periodic elastomer structures, Internat. J. Solids Structures 49 (19) (2012) 2881–2885.
[26] K. Bertoldi, M.C. Boyce, Wave propagation and instabilities in monolithic and periodically structured elastomeric materials undergoing large deformations, Phys. Rev. B: Condens. Matter Mater. Phys. 78 (18) (2008) 4107–4122.
[27] J.H. Jang, C.Y. Koh, K. Bertoldi, M.C. Boyce, E.L. Thomas, Combining pattern instability and shape-memory hysteresis for phononic switching, Nano Lett. 9 (5) (2009) 2113–2119.
[28] J. Shim, P. Wang, K. Bertoldi, Harnessing instability-induced pattern transformation to design tunable phononic crystals, Internat. J. Solids Struct. 58 (2015) 52–61.
[29] S. Babaee, P. Wang, K. Bertoldi, Three-dimensional adaptive soft phononic crystals, J. Appl. Phys. 117 (2015) 244903.
[30] S. Babaee, N. Viard, P. Wang, N.X. Fang, K. Bertoldi, Harnessing deformation to switch on and off the propagation of sound, Adv. Mater. 28 (2016) 1631–1635.
[31] E.G. Barnwell, W.J. Parnell, I.D. Abrahams, Antiplane elastic wave propagation in pre-stressed periodic structures; tuning, band-gap switching and invariance, Wave Motion 63 (2016) 98–110.
[32] W.J. Parnell, Nonlinear pre-stress for cloaking from antiplane elastic waves, Proc. Roy. Soc. A: Math. Phys. Engrg. Sci. 468 (2138) (2012) 563–580.
[33] W.J. Parnell, A.N. Norris, T. Shearer, Employing pre-stress to generate finite cloaks for antiplane elastic waves, Appl. Phys. Lett. 100 (17) (2012) 171907.
[34] A.N. Norris, W.J. Parnell, Hyperelastic cloaking theory: transformation elasticity with pre-stressed solids, Proc. Roy. Soc. A: Math. Phys. Engrg. Sci. 468 (2146) (2012) 2881–2903.
[35] W.J. Parnell, T. Shearer, Antiplane elastic wave cloaking using metamaterials, homogenization and hyperelasticity, Wave Motion 50 (7) (2013) 1140–1152.
[36] Y. Fu, R. Ogden, Nonlinear Elasticity: Theory and Applications, Cambridge University Press, 2001.
[37] M. Levinson, I. Burgess, A comparison of some simple constitutive relations for slightly compressible rubber-like materials, Int. J. Mech. Sci. 13 (6) (1971) 563–572.
[38] R.W. Ogden, Non-Linear Elastic Deformations, Dover, 1998.
[39] M.S. Kushwaha, P. Halevi, G. Martinez, Theory of acoustic band structure of periodic elastic composites, Phys. Rev. B: Condens. Matter Mater. Phys. 49 (4) (1994) 2313–2322.